

Carleman-Grad approach to the quantum simulation of fluids

Claudio Sanavio* and Sauro Succi
*Fondazione Istituto Italiano di Tecnologia
Center for Life Nano-Neuroscience at la Sapienza
Viale Regina Elena 291, 00161 Roma, Italy*

Enea Mauri
*Fondazione Bruno Kessler
Via Sommarive 18, 38123, Povo (TN), Italy and
Fondazione Istituto Italiano di Tecnologia
Center for Life Nano-Neuroscience at la Sapienza
Viale Regina Elena 291, 00161 Roma, Italy*
(Dated: June 4, 2024)

We discuss the Carleman linearization approach to the quantum simulation of classical fluids based on Grad’s generalized hydrodynamics and compare it to previous investigations based on lattice Boltzmann and Navier-Stokes formulations. We show that the Carleman-Grad procedure exhibits intermediate properties between the two. Namely, convergence of the Carleman iteration over a few tens of timesteps and a potentially viable quantum circuit implementation using quantum linear algebra solvers. However, both features still need substantial improvements to yield a viable quantum algorithm for fluid flows.

I. INTRODUCTION: QUANTUM COMPUTING FOR FLUIDS

In recent years there has been a growing interest in exploring the potential of quantum computing for nonlinear problems in classical physics, and most notably the physics of fluids [1–5].

The potential of quantum computing for fluid flows is indeed mind-boggling [6, 7], as readily appreciated by considering that the computational complexity of a turbulent flow at Reynolds number Re scales like Re^3 . Hence, using amplitude encoding, it requires a number of qubits

$$Q(Re) = 3 \log_2 Re \sim 10 \log_{10} Re. \quad (1)$$

Current near-exascale electronic supercomputers can reach up to $Re \sim 10^7$ (a standard automobile), meaning $Q \sim 70$, which is well within the *nominal* capabilities of current quantum hardware [8]. Clearly, the optimistic relation described by Eq. (1) needs to be scaled up by a factor of ten to a hundred, to acknowledge the gap between nominal (logical) qubits and functional (physical) ones, raising the count to $Q \sim 10^3 \div 10^4$. While still beyond the capabilities of current quantum computers, this looks like a plausible target for the near to mid-term future.

However, when it comes to fluids, in addition to handling decoherence and quantum noise, one has to devise suitable strategies to deal with two distinctive features with no counterpart in (standard) quantum mechanics: nonlinearity and dissipation. Many such strategies have been proposed over the last few years, but no clearcut solution has emerged yet [5]. For instance, in [2] a quantum ODE solver is proposed, but no specific implementation of the quantum oracle is presented. Another interesting possibility is to adapt variational quantum eigenvalue solvers to the fluid equations, to sidestep the difficult issue of time marching. However, to date, it appears difficult to minimize the associated functional at the required level of accuracy [9] for quantitative fluid dynamic purposes.

Another promising approach is the one based on Carleman linearization [10–12], whereby the finite-dimensional nonlinear fluid problem is turned into an infinite-dimensional linear one, to be truncated at a suitable level of the hierarchy.

This is the method discussed in the present paper.

II. CARLEMAN LINEARIZATION OF THE LOGISTIC EQUATION

We begin by presenting the main ideas behind Carleman linearization by means of a simple pedagogical example in zero spatial dimensions, namely the following logistic equation:

* claudio.sanavio@iit.it

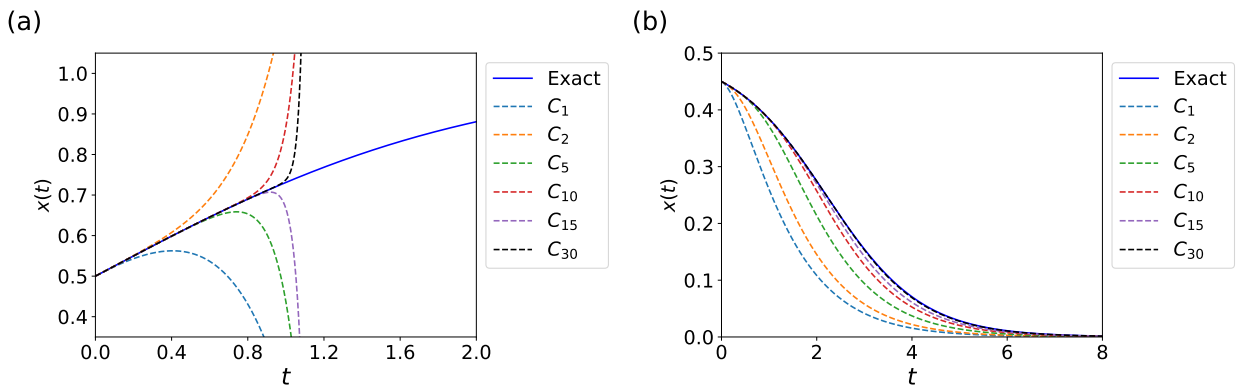


FIG. 1. Convergence of the Carleman Linearization for the logistic equation at increasing orders of the truncation. (a) The growing logistic equation, with $a = -1, b = -1$ and initial condition $x_0 = 0.5$. (b) The decaying logistic equation, with $a = 1, b = 1$ and initial condition $x_0 = 0.45$.

$$\dot{x} = -ax + bx^2, \quad x(0) = x_0 \quad (2)$$

where $a > 0$ is the decay rate and $b > 0$ is the quadratic regeneration rate.

This equation admits a stable attractor $x_s = 0$ and an unstable one $x_u = 1/R$, where $R = b/a$. Hence, any initial condition such that $0 < Rx_0 < 1$ is asymptotically attracted to 0, whereas for $Rx_0 > 1$, the solution blows up in a finite time $t_{sing} = a^{-1} \log(\frac{Rx_0}{Rx_0-1})$, as it is readily inferred by inspecting the exact solution:

$$x(t) = x_0 \frac{e^{-at}}{1 - Rx_0(1 - e^{-at})}, \quad (3)$$

For the case $a < 0$ and $b < 0$, the attractors swap their role: $x_u = 0$ becomes unstable and the stable one is $x_s = 1/R$. Hence any initial condition $x_0 > 0$ is attracted to $1/R$, while any $x_0 < 0$ would diverge to minus infinity in a finite time. It has to be noted that the decaying case, $a, b > 0$ and the growing one $a, b < 0$ turn one into another under the dual transformation $x' = 1/R - x$. Hence they are basically equivalent.

The Carleman procedure consists in renaming $x^{(1)} \equiv x$ and $x^{(2)} \equiv x^2$, so that the logistic equation takes the linear form

$$\dot{x}^{(1)} = -ax^{(1)} + bx^{(2)}, \quad (4)$$

with the equation for $x^{(2)}$ given by

$$\dot{x}^{(2)} = 2x\dot{x} = -2ax^{(2)} + 2bx^{(3)}, \quad (5)$$

where we defined $x^{(3)} \equiv x^3$. Iterating the procedure to the k -th order delivers:

$$\dot{x}^{(k)} = -k(ax^{(k)} - bx^{(k+1)}). \quad (6)$$

This is an endless hierarchy, which is then truncated at a given order K by setting $x^{K+1} = 0$, in the hope that the truncated solution can still capture the essential behaviour of the exact one over the desired timespan.

In practice, it can be shown that the Carleman hierarchy is just another way of representing the exact solution as an infinite power series in the term $Rx_0(1 - e^{-at})$. In fact, the truncation at order K yields the solution

$$x(t) = x_0 e^{-at} \sum_{k=0}^K \left[Rx_0(1 - e^{-at}) \right]^k. \quad (7)$$

In the stable regime, $Rx_0 < 1$, higher truncation levels result in a better approximation, as shown in Fig. 1(b), with parameters set $a = 1, b = 2$ and $x_0 = 0.45$.

The growing case, albeit analytically equivalent under the duality transformation mentioned earlier on, shows a different behaviour. It is straightforward to see that for the growing case $a, b < 0$, the radius of convergence of the series in Eq. (7) is given by

$$t_{\text{lim}} = \frac{1}{|a|} \log \left(\frac{1 + Rx_0}{Rx_0} \right). \quad (8)$$

This behaviour is shown in Fig. 1(a) for the case $a = -1, b = -1, x_0 = \frac{1}{2}$, where each successive iteration expands the time horizon of convergence, until the time horizon $t_{\text{lim}} = \log(3) \sim 1.098$ is reached. As mentioned earlier on, the decaying and growing cases are dual, but the Carleman procedure is not able to catch this equivalence, since the growing case is restricted by the convergence radius of the series (7). As a result, the Carleman expansion fails to capture the saturation regime.

Despite its simplicity, the logistic equation provides a few useful hints for the Carleman linearization of the fluid equations. First, like fluids, it presents a quadratic non-linearity. Second, it shows that the time horizon of the Carleman series around an unstable attractor depends on the strength of the nonlinearity via the dimensionless group Rx_0 , namely the ratio of the initial to the time asymptotic condition $1/R$. Third, the logistic equation bears a close similarity to the collision operator of kinetic equations. This observation prompted the earliest attempts to apply the Carleman procedure to the lattice formulation of fluids, as we describe next.

Besides these similarities, there are also a number of caveats to this analogy, which deserves to be discussed in some detail in view of some confusing results in the previous literature.

To begin with, it should be appreciated that the Carleman results for the logistic equation cannot be carried over as-is to the case of the fluid equations, the reason being that in the latter, the attractor is generally non-local due to spatial coupling due to advection and diffusion. This is readily shown already for the simplest case of the Burgers equation (pressure-less fluid), by casting this equation in relaxation form:

$$\partial_t u = \Delta \left(u - \frac{Re}{2} \Delta^{-1} \nabla u^2 \right) \quad (9)$$

Δ^{-1} being the Green function of the Laplacian operator and ∇ the gradient operator. Since the Green function is nonlocal, it is clear that the quadratic non-linearity of the Burgers equation, once cast in relaxation form, leads to a global attractor

$$u^{eq} = \frac{Re}{2} \Delta^{-1} \nabla u^2 \quad (10)$$

This is likely to explain why the Carleman-Burgers procedure does not abide by the restriction $Re < \sqrt{2}$ advocated in the theorem proposed in [13]. It is also worth further noting that this theorem was derived from inspection of the unstable attractor of the logistic equation a situation which does not relate directly to the physics of fluids since even though the local equilibrium u^{eq} can grow in time under a physical instability, the flow configuration u still is attracted to it, as the Green function of the Laplacian is negative-definite. We conclude that the restriction $Re < \sqrt{2}$ is not relevant to the Carleman linearization of the fluid equations.

III. CARLEMAN LATTICE BOLTZMANN VERSUS CARLEMAN NAVIER-STOKES

The satisfactory convergence of the Carleman procedure applied to the logistic equation points to the Lattice Boltzmann (LB) method as a natural candidate for a fluid implementation (full details in the original publications [11, 12]). Additionally, the LB method is known for its efficient use of parallel resources, making it a competitive tool for large-scale fluid dynamics simulations [14, 15].

To illustrate the point, let us remind the basic form of the LB equation:

$$f_i(\vec{x} + \vec{c}_i, t + 1) - f_i(\vec{x}, t) = -\omega(f_i(x, t) - f_i^{eq}(x, t)) \quad (11)$$

where $f_i(\vec{x}, t)$ is the probability of finding a representative fluid particle (discrete Boltzmann distribution function) at site \vec{x} and time t , with a given molecular velocity \vec{c}_i , where i runs over a discrete lattice with suitable symmetry [16]. In the above, the timestep has been set to unity for simplicity. The left-hand side is the free streaming, whereas the right-hand side encodes collisions in the form of a relaxation to a local equilibrium f_i^{eq} on a timescale $\tau = 1/\omega$. The local equilibrium takes the following form:

$$f_i^{eq} = w_i \left(\rho + \frac{\vec{J} \cdot \vec{c}_i}{c_s^2} + \frac{\rho^{-1} \vec{J} \cdot \vec{J} (\vec{c}_i \cdot \vec{c}_i - c_s^2)}{2c_s^4} \right) \quad (12)$$

where $\rho = \sum_i f_i$ is the fluid density and $\vec{J} = \sum_i f_i \vec{c}_i$ is the fluid current density. The collision operator bears a strong resemblance to the logistic equation in that not only it is quadratic but it is also local, a property that is not and cannot be shared by the Navier-Stokes equations, since it derives explicitly from the extra velocity dimensions of phase-space [17].

Moreover, since the fluid current is a local collisional invariant, the Carleman procedure based on such quantity instead of the discrete distribution, is captured *exactly* by a second order Carleman procedure [18]. Unfortunately, this beautiful property is broken by the streaming operator, although one may expect that a remnant of this convenient property may remain also in the space-dependent case.

Importantly, as first noted in [19], in the LB method the strength of the nonlinearity is formally measured by the Mach number instead of the Reynolds number. The reason is twofold; first, the local equilibria are quadratic in the Mach number, second, the LB formalism does not involve any second order derivative in space because dissipation emerges out of local relaxation. The latter is again a distinctive property of the LB scheme: information always travels along straight lines, constant in space in time, regardless of the complexity of the flow field. As a result, the expectation is that Carleman-LB (CLB) should meet with a much lower nonlinearity barrier as compared to the Carleman-Navier-Stokes (CNS) procedure.

In Refs. [11] and [12] we applied CLB and CNS respectively. The two formulations led to very different results. In both cases, we simulated a two-dimensional Kolmogorov-like flow, defined on a $L \times L$ square lattice with the following initial conditions for the lattice site $\vec{x} = (x_1, x_2)$:

$$\rho(\vec{x}, 0) = 1, \quad (13)$$

$$J_1(\vec{x}, 0) = A_1 \cos kx_2, \quad (14)$$

$$J_2(\vec{x}, 0) = A_2 \cos kx_1, \quad (15)$$

where J_a , with $a = 1, 2$, is the fluid current density in the two dimensional plane and the wavenumber is set to $k = 2\pi/L$. We simulated the dynamics on a 32×32 grid with periodic boundary conditions and we compared the solutions for the macroscopic quantities ρ, \vec{J} obtained by the CLB and by the CNS procedures. By modifying the value of the amplitudes A_1, A_2 , we explored different regimes of nonlinearity.

In fact, if either A_1 or A_2 is set to zero, the nonlinear terms of the fluid equation vanish by construction. In this case, the current J_a decays exponentially in time as

$$J_{1,2}(\vec{x}, t) = J_{1,2}(\vec{x}, 0)e^{-\nu k^2 t}, \quad (16)$$

with ν being the kinematic viscosity.

We set the viscosity to $\nu = 1/6$, the amplitude to $U = A_1 = A_2 = 0.1$ and $L = 32$, yielding $Re = \frac{UL}{\nu} \sim 20$. The CLB numerical simulations provided three-digit convergence up to about 100 timesteps, even with the lowest Carleman truncation, namely second order. This is shown in Fig. 2, where we plot the relative error ϵ_L , defined as

$$\epsilon_L = \sum_{a=1,2} \left| \frac{J_a^{\text{LBM}} - J_a^{\text{CLB}_2}}{J_a^{\text{LBM}}} \right|, \quad (17)$$

which accounts for the difference between the values of \vec{J} obtained with direct numerical simulation of the LBM and the value obtained by Carleman-LB linearization. The relative error is plotted at two different times, $t = 1$ and $t = 10$, and it is found to stabilize at larger times.

By contrast, by using CNS, we have not been able to preserve a similar accuracy beyond a time horizon of a few time steps, (with $dt = 0.01$), even at fourth order in the Carleman truncation. The relative error ϵ_N defined in a similar manner as Eq. (17) for the CNS method is plotted in Fig. 3 for the same times $t = 1$ and $t = 10$. As one can appreciate, at time $t = 10$ the CNS error is about thirty times larger than the CLB error.

Although much more validation work is needed to put these preliminary observations on firm ground, these numerical results are fairly consistent with the theoretical perspective discussed earlier on in this paper, namely that LB should be much more amenable to Carleman linearization than the Navier-Stokes equations.

As commented above, the stream-relax structure of the LB method brings about very substantial advantages, primarily a Mach-controlled nonlinearity as well as unitarity, to be discussed shortly.

However, the excellent properties of LB come at a steep price, non-locality, as we are going to comment in the next section.

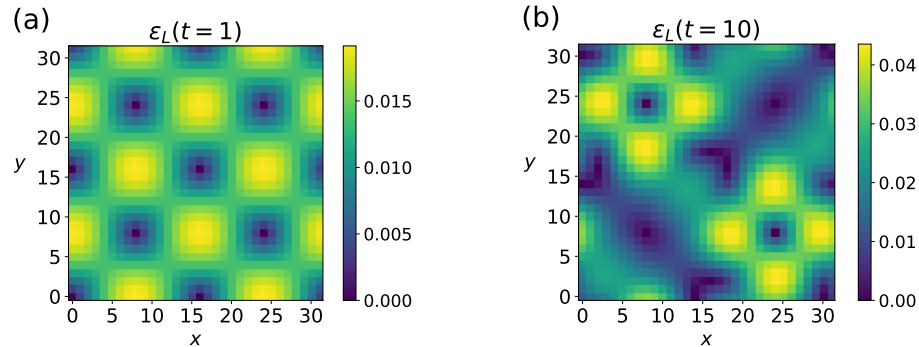


FIG. 2. The relative error (17) of the CLB method truncated at second order on each site of a 32×32 lattice, for a Kolmogorov-like flow with initial conditions $A_1 = A_2 = 0.1$, $\nu = 1/6$.

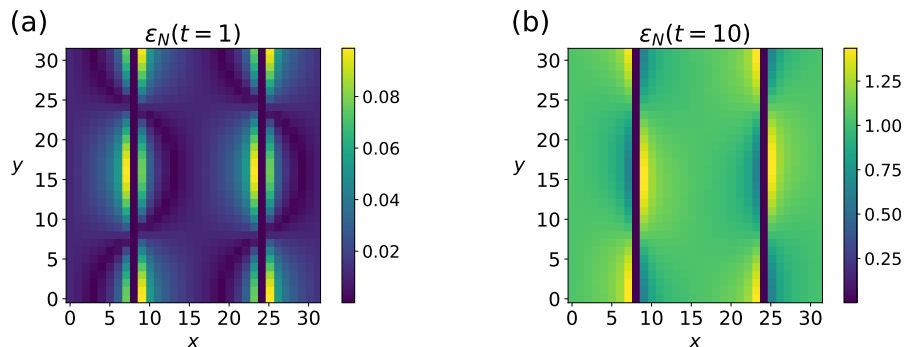


FIG. 3. The relative error (17) of the CNS method truncated at second order on each site of a 32×32 lattice, for a Kolmogorov-like flow with initial conditions $A_1 = A_2 = 0.1$, $\nu = 1/6$.

A. Nonlocality

A major shortcoming of the Carleman procedure is the exponential growth of the number of variables with the order of the Carleman expansion. Let f_i , $i = 1, b$ the number of CLB variables at level 1 for a LB scheme with b discrete velocities \vec{c}_i , with $b = 9$ in two spatial dimensions and $b = 19$ in three. In a local scheme, the Carleman variables at level two are $f_{ij} = f_i f_j$, hence $b(b+1)/2$ components, while at level k the total number of CLB variables is:

$$N_{CLB}(k) = b + b(b+1)/2 + \dots + b(b+1) \dots (b+k)/k! \sim b^k. \quad (18)$$

As an example, the two cases $b = 9$ and $b = 19$ up to $k = 10$ are reported in table I, along with the corresponding number of required qubits.

As one can see, the number of required qubits grows less than linearly with the number of Carleman levels, and remains fairly moderate up to level 10, which is taken here as an upper bound for satisfactory Carleman convergence.

Clearly, locality is key to this favourable scaling. If, on the other hand, the Carleman scheme involves Carleman variables sitting at different lattice sites, say $f_{ij}(\vec{x}_i, \vec{x}_j)$, then the number of Carleman variables after T timesteps scales like $(Tb)^k$ instead of b^k . Since T scales at least linearly with the linear size of the domain, even moderate grid sizes, say $G \sim 10^6$ in three spatial dimensions, quickly lead to unviable schemes.

Unfortunately, CLB appears to be inherently nonlocal, since, by construction, different populations, say $f_i(\vec{x}, t)$ and $f_j(\vec{x}, t)$ at the same location \vec{x} at time t , free-stream to different locations, $\vec{x}_i = \vec{x} + \vec{c}_i$ and $\vec{x}_j = \vec{x} + \vec{c}_j$ at time $t + 1$, thus generating a non-local pair $f_{ij}(\vec{x}_i, \vec{x}_j, t + 1)$.

In this respect, CNS fares better because, by using conservative differencing in space, locality can be preserved at all Carleman levels [12]. However, as discussed above, the CNS method shows too poor convergence to offer a viable solution for the quantum simulation of fluids.

k	N_9	Q_9	N_{19}	Q_{19}
1	9	4	19	5
2	54	6	209	8
3	219	8	1539	11
4	714	10	8854	14
5	2001	11	42503	16
6	5004	13	177099	18
7	11439	14	657799	20
8	24309	15	220074	22
9	48619	16	6906899	24
10	92377	17	20030009	26

TABLE I. Number of Carleman variables and corresponding number of qubits for the cases $b = 9$ and $b = 19$, respectively.

Given such a state of affairs, we set out to explore a third avenue, the Carleman-Grad (CG) approach, in the hope it may combine the good convergence of CLB with the locality of CNS.

IV. GRAD'S GENERALIZED HYDRODYNAMICS

The basic idea of Grad generalized hydrodynamics is to take progressive moments of the Boltzmann probability distribution and inspect the resulting open hierarchy of hyperbolic PDEs. Grad's thirteen-moment method is a technique to derive solutions of the Boltzmann equation in fluid-like regimes beyond the realm of Navier-Stokes hydrodynamics [16, 20]. Formally, it amounts to projecting the Boltzmann equation upon a suitable set of basis functions in velocity (momentum) space, typically tensor Hermite polynomials for the case of cartesian coordinates. The expansion is truncated to third order terms, delivering the equations of motion for the fluid density $\rho = \int f d^3v$, the fluid current $J_a = \int f v_a d^3v$, the momentum flux tensor $P_{ab} = \int f v_a v_b d^3v$, and the energy flux $Q_{abc} = \int v_a v_b v_c d^3v$, with latin indexes running over the spatial dimensions.

This delivers the following set of hyperbolic equations:

$$\partial_t \rho + \partial_a J_a = 0 \quad (19)$$

$$\partial_t J_a + \partial_b P_{ab} = 0 \quad (20)$$

$$\partial_t P_{ab} + \partial_c Q_{abc} = -\omega(P_{ab} - P_{ab}^{\text{eq}}), \quad (21)$$

This system of equations generalizes the Navier-Stokes equations (NSE) in that all physical signals travel at finite speed, as opposed to the parabolic character of the dissipative term of the NSE.

Like for LB, the NSE are recovered in the limit of weak departure from local equilibrium. Under such limit, the third equation can be closed by assuming adiabatic relaxation of P_{ab} to its local equilibrium, namely:

$$P_{ab} \sim P_{ab}^{\text{eq}} - \tau \partial_c Q_{abc}^{\text{eq}} \quad (22)$$

where $\tau = 1/\omega$ and the equilibrium tensors read as follows:

$$\begin{aligned} P_{ab}^{\text{eq}} &= \frac{J_a J_b}{\rho} + c_s^2 \rho \delta_{ab} \\ Q_{abc}^{\text{eq}} &= c_s^2 (J_a \delta_{bc} + J_b \delta_{ac} + J_c \delta_{ab}), \end{aligned} \quad (23)$$

where c_s is the speed of sound.

Note that in the latter we have neglected cubic nonlinearities by assuming low-Mach number conditions.

The appeal of the Grad formulation rests with its hyperbolic character, which reflects in the conservative nature of the equations, hence the locality of the discretized scheme. In addition, the number of native variables is $1+3+6 = 10$, half than CLB.

Despite its conceptual and mathematical elegance, Grad's method suffers a major drawback: lack of realizability, i.e. it does not ensure the positive definiteness of the truncated distribution function, often reflecting instability issues.

Regularization techniques have been developed over the years which permit to describe several far-from-equilibrium transport phenomena as they typically arise in the context of rarefied gas dynamics [21]. Hence, the regularized CG scheme could form the basis to simulate these problems on quantum computers, offering an alternative to expensive Monte Carlo procedures.

A. Grad versus Lattice Boltzmann

It is worth recapping the points of commonality and departure between Grad and Lattice Boltzmann.

Commonalities: i) they are both first order in space and time, ii) dissipation emerges from local relaxation with no need of second order spatial derivatives, iii) the nonlinearity is local, hence formally measured by the Mach number instead of the Reynolds number.

Point of departure: they differ in the structure of spatial transport. The key point is that, at variance with the fluid equations, the LB information invariably travels along straight characteristics, $d\vec{x}_i = \vec{c}_i dt$, constants in space and time. As a result, the left-hand side of the LB equation is exact, a property that lies at the heart of the success of the LB method for classical fluids. In the CLB context, this means that the streaming operator remains unitary also upon lattice discretization. Indeed, the collisionless LB update ($\omega = 0$) is simply the identity $f_i(\vec{x} + \vec{c}_i, t + 1) = f_i(\vec{x}, t)$, a property which can be shown to hold at all Carleman levels. In the Grad method, however, fluid transport is implemented via first-order spatial derivatives of the generalized currents. Hence, besides being subject to discretization and round-off errors, such discrete derivatives do not preserve unitarity under Euler time marching. In this respect, the Grad method aligns with the Navier-Stokes equations.

With all these plus and minuses factored in, the question remains as to whether the Grad formulation can benefit from the excellent convergence of CLB, while sharing the locality of the CNS formulation. In the following we investigate such question by first formulating the Carleman-Grad procedure and then by performing numerical simulations.

V. THE CARLEMAN-GRAD PROCEDURE

The first order Carleman step is to set the nonlinear terms $J_{ab} = 0$ and $J_{abc} = 0$. Further Carleman steps require knowledge of J_{ab} to compute P_{ab}^{eq} . The dynamic equation for J_{ab} can be obtained the same way as for CNS, with the advantage of more locality since no Laplacian operators are involved.

In order to apply the Carleman linearization and conserve the local form of the equations at all Carleman orders, we proceed as follows. First we use the approximation valid for a weakly-compressible flow $\rho^{-1} \approx 2 - \rho$, in order to express all the equations (19)–(21) in polynomial form. We collect all the local variables in a vector $V(\vec{x}, t) = (\rho, J_a, P_{ab})$, with a, b running over the spatial dimensions, and rewrite Eqs. (19)–(21) in matrix form as:

$$\partial_t V(\vec{x}, t) = \hat{L}_1 V(\vec{x}, t) + \hat{L}_2 V^{(2)}(\vec{x}, t) + \hat{L}_3 V^{(3)}(\vec{x}, t), \quad (24)$$

where the matrices \hat{L}_j , with $j = 1, 2, 3$ multiply the linear, quadratic and cubic terms respectively. Note that the matrices \hat{L}_2 and \hat{L}_3 are very sparse, since the non-zero terms come only from the equilibrium tensor P_{ab}^{eq} (23). Their explicit form can be found in the Appendix.

Here we explicitly apply the Carleman procedure up to third order, thus ignoring the terms $V^{(k)}$, with $k > 3$, but the generalization is straightforward for higher truncation orders. We discretize time via the Euler forward scheme, yielding the following relation for each local vector:

$$V_a(\vec{x}, t + 1) = A_{ab} V_b(\vec{x}, t) + B_{abc} V_{bc}^{(2)}(\vec{x}, t) + C_{abcd} V_{bcd}^{(3)}(\vec{x}, t), \quad (25)$$

where we have defined $A = \mathbb{1} + dt\hat{L}_1$, $B = dt\hat{L}_2$ and $C = dt\hat{L}_3$. The second and third-order Carleman variables are the tensor products of the local vectors,

$$V^{(2)}(\vec{x}, t) = V(\vec{x}, t) \otimes V(\vec{x}, t), \quad (26)$$

and their evolution can be obtained by tensor product of Eq. (25) as

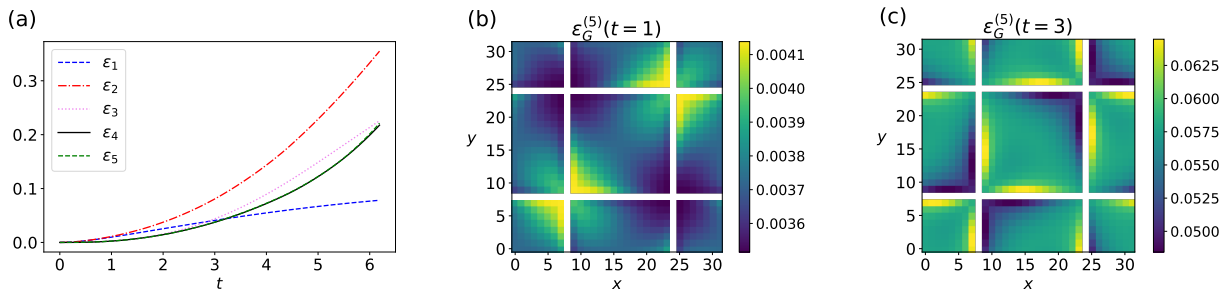


FIG. 4. (a) The time evolution of the relative errors ϵ_k of the CG method truncated at order k averaged over the lattice gridpoints, for a Kolmogorov-like flow with initial conditions $A_1 = A_2 = 0.1$, and $\omega = 2$. (b) The relative error of the CG method with $k = 5$ plotted at each lattice site at time $t = 1$. (c) The relative error of the CG method with $k = 5$ plotted for each lattice site at time $t = 3$. The points on the white bands are removed from the plot since J was initialized to 0.

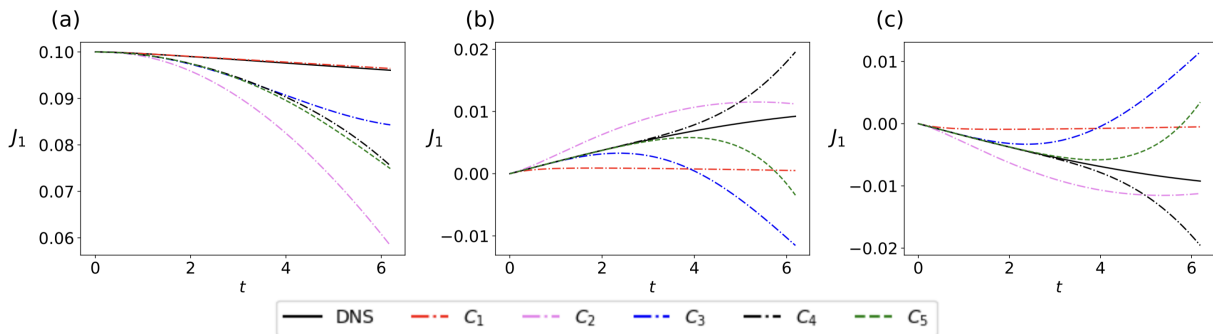


FIG. 5. The time evolution of the current density J of the CG method truncated at different orders k for specific representative lattice gridpoints, for a Kolmogorov-like flow with initial conditions $A_1 = A_2 = 0.1$, $\omega = 2$ and $dt = 0.01$. The speed of sound is set $c_s = \frac{1}{\sqrt{3}}$. The chosen points are $\vec{x}_a = (0, 0)$, $\vec{x}_b = (8, 0)$ and $\vec{x}_c = (8, 16)$ in (a), (b) and (c) respectively.

$$\begin{aligned}
 V^{(2)}(\vec{x}, t+1) &\equiv V(\vec{x}, t+1) \otimes V(\vec{x}, t+1) \\
 &= (A \otimes A)V^{(2)}(\vec{x}, t) + (B \otimes A + A \otimes B)V^{(3)}(\vec{x}, t), \\
 V^{(3)}(\vec{x}, t+1) &= (A \otimes A \otimes A)V^{(3)}(\vec{x}, t)
 \end{aligned} \tag{27}$$

and all the higher orders terms are neglected.

VI. CARLEMAN-GRAD: NUMERICAL RESULTS

Next, we show the results obtained with the CG method up to order 5 for the simulation of the Kolmogorov-like flow described in Sec. III. In Fig. 4(a) we show the mean value ϵ_k of the relative error $\epsilon_G^{(k)}$, for the CG linearized system truncated at order k , obtained by averaging over the entire set of gridpoints. In Figs. 4(b) and 4(c) we show the relative error at each site of the lattice for $k = 5$ at $t = 1$ and $t = 3$, respectively. The latter is chosen since the first and the fifth order approximation yield the same value of ϵ_k .

Figures 5(a)-(c) compare the values of J_1 obtained from CG dynamics at different orders with those obtained from direct numerical simulation (DNS) of Grad's equations at three lattice sites: $\vec{x} = (0, 0)$, $\vec{x} = (8, 0)$, and $\vec{x} = (8, 16)$, respectively.

Each curve exhibits a distinct behaviour and convergence times. At $\vec{x} = (0, 0)$, the dominant dynamics leads to a current decay, hence the first-order Carleman truncation best captures the dynamics at later times, even though higher-order approximations are initially more accurate. In contrast, at points $\vec{x} = (8, 0)$ and $\vec{x} = (8, 16)$, the convergence times for the fourth and fifth-order CG dynamics are similar, mirroring the behaviour observed in Fig. 1(a) for the growing logistic equation. We speculate that such similarity may point to the existence of a suitable transformation of

the Carleman variables more conducive to a convergent solution. For instance, one could write a dual Navier-Stokes equation for $u^{eq} - u$, where u^{eq} is the nonlocal equilibrium discussed in the early part of this paper, a possibility that remains to be explored in the future.

VII. TIME MARCHING, UNITARITY, AND DEPTH OF THE QUANTUM CIRCUIT

In this section, we analyze the time marching scheme to solve the Carleman linearized evolution problem:

$$\frac{dV^{(k)}}{dt} = C_k V^{(k)}, \quad k = 1, K \quad (28)$$

where $V^{(k)}$ is the array of Carleman variables at level k of the procedure and C_k is the corresponding Carleman matrix.

A. Single-step telescopic Euler scheme

Time marching is a notoriously hard issue on quantum computers, due to the measurement problem: the updated state at time $t + dt$ cannot be copied into the initial state for the next time step, since this would require a full-state tomography of complexity $\mathcal{O}(4^Q)$.

This problem can be circumvented by adopting a single-step telescopic forward Euler scheme:

$$V^{(k)}(t) = (\mathbb{1} - C_k \Delta t)^T V^{(k)}(0) \quad (29)$$

where $t = T\Delta t$ and $\mathbb{1}$ is the identity matrix.

The above scheme propagates the initial condition at $V^{(k)}(0)$ to the final state at $V^{(k)}(t)$ in a single large step of size t with the same accuracy of T timesteps of size $dt = t/T$, so as to avoid any intermediate measurement. Of course, this does not come for free. In fact, if the C_k matrix has a bandwidth B_k , the telescopic propagator has bandwidth TB_k , hence, for any T comparable with the linear size of the domain, this amounts to a full matrix even in the case of a sparse matrix C_k .

We further note that the matrix C_k consists of a unitary streaming component and a non-unitary one, in the form of a local collision-relaxation operator for CLB and a Laplacian operator for CNS.

In the CLB scheme we chose to represent the collision matrix as a weighted superposition of two unitaries, according to the procedure first discussed in [22]. This has the merit of simplicity, but it comes at a price. Indeed, by writing the collision matrix as a weighted sum of two unitaries, the corresponding single-step quantum circuit update fails with a non-zero probability $p_f(\gamma) > 0$. Hence the failure probability over a sequence of T timesteps is p_f^T , meaning that in order to keep the multistep failure probability well below 1, optimal values of γ must be found such that

$$p_f(\gamma) < 1/T.$$

The best value we have found to date for CLB is $p_f \sim 0.09$, which allows us to propagate about 10 steps with an acceptance ratio of about 1/3. Clearly, smaller values of p_f are needed to advance over hundreds or thousands of timesteps.

We note, however, that such a restriction could be sidestepped by turning to quantum linear algebra solvers, to which we shall return in the final part of this paper.

It is also important to notice that, even in the case where the continuum problem, Eq. (28), is unitary, the Euler scheme, Eq. (29), is generally not. However, contrary to CNS, CLB does preserve unitarity of the streaming operator. Finally, we inspect the depth of the quantum CLB algorithm, namely the number of two qubits gates required to implement the CLB telescopic operator.

To date, we have not been able to find any CLB matrix representation leading to a circuit depth below the upper-bound value 4^Q . Indeed, projection over a tensorial basis of native quantum gates delivers an exponentially long series, whose coefficients do not show any significant decay in amplitude over the entire basis set. In this respect, the CLB matrix appears as irreducible as a generic unitary, thus compromising the viability of CLB scheme, despite its excellent convergence properties. If one could find a reducible representation, then CLB would turn up into a serious candidate for the quantum simulation of fluids, but for the moment it is not. On the other hand, CNS offers no alternative, due to its very poor Carleman convergence and CG sits in a sort of intermediate position.

Next, we present our perspectives for a quantum implementation of CG.

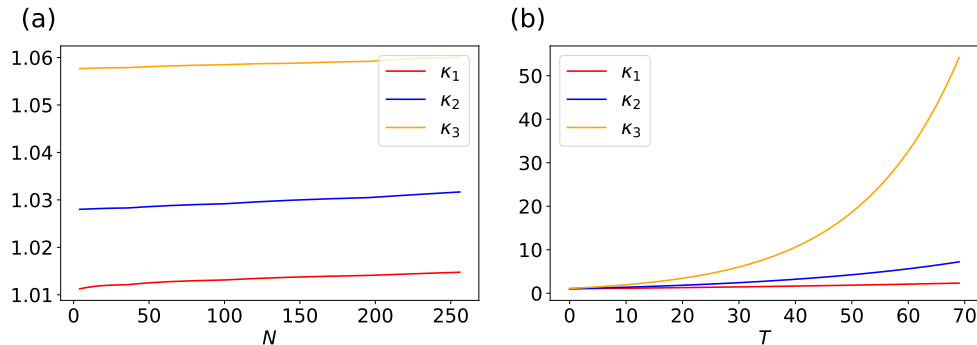


FIG. 6. (a) The condition number κ of the Carleman matrix C_k with truncation order $k = 1, 2$ and 3 varying the number of lattice sites. (b) The condition number κ of the Carleman matrix C_k with truncation order $k = 1, 2$ and 3 as a function of the number of timesteps. The parameters of the CG matrix have been set to $\omega = 2$ and $dt = 0.01$.

B. Perspectives for a Carleman-Grad quantum circuit based on quantum linear solvers

The local formalism introduced with Eqs. (27) for the Grad-method leads to a matrix characterized by low sparsity. This property is crucial for the implementation of an efficient quantum circuit reproducing the behaviour of the Carleman matrix [23, 24].

In fact, considering the simple case $k = 2$, the evolution of the global Carleman array

$$\vec{V} = \left(V(\vec{x}_1), \dots, V(\vec{x}_N), V^{(2)}(\vec{x}_1), \dots, V^{(2)}(\vec{x}_N) \right) \quad (30)$$

for a lattice with N gridpoints and a single time step dt , writes as follows:

$$\vec{V}(t + dt) = \begin{pmatrix} \hat{A} & \hat{B} \\ 0 & \hat{A} \otimes \hat{A} \end{pmatrix} \vec{V}(t), \quad (31)$$

where the matrices \hat{A}, \hat{B} are given in Appendix A.

In order to solve the linear system of equations (28) we refer to two quantum linear solvers.

The first is the algorithm proposed by Harrow, Hassidim, and Lloyd (HHL) [25], featuring a computational complexity $\mathcal{O}(\log[g^k N] s^2 \kappa^2 / \epsilon)$, where κ is the condition number of C_k and ϵ is the desired precision. The second, is the quantum solver proposed by Childs, Kothari, and Somma (CKS) [26] which improves the HHL algorithm by reducing the computational complexity to $\mathcal{O}(\log[g^k N / \epsilon] \kappa)$.

Although the CKS algorithm consistently improves the dependency on ϵ , its implementation necessitates a black-box oracle Hamiltonian to replicate the matrix C_k , thereby severely hampering its practical application. By contrast, the HHL algorithm is more readily applicable, at least in principle, to the present investigations.

The sparsity s of the Carleman matrix C_k of Eq. (28) for the local Grad system scales 6^k , to be compared with the size of the matrix C_k itself, namely $6^k N \times 6^k N$. Note that the $\log N$ quantum advantage of both HHL and CKS algorithms can be totally spoiled by an unfavourable dependency of the condition number $\kappa(N)$ [27] with the number of sites.

To investigate this point, we have explicitly calculated the value of κ as a function of N for the case $\omega = 2$ and found a sub-linear dependence on N , as reported in Fig. 6(a).

In order to obtain the solution at a given time t , we need to apply the Carleman matrix to the initial vector state $T = t/dt$ times, with $\vec{V}(t) = C^T \vec{V}(0)$. In Fig. 6(b) we plot the condition number as a function of the number of time steps, $\kappa(T)$, for the case $\omega = 2, dt = 0.01$ and show that it exhibits a polynomial dependence on T . As a result, the trend of κ with both N and T justifies some optimism for future quantum implementations of the CG method, provided convergence and circuit depth can be kept under control.

To date, we have not been able to address the other key requirement of an efficient quantum implementation of the Carleman matrix: block-diagonality [23]. This leaves us again with a 4^Q depth of the CG quantum circuit, like for CLB.

Further investigations are needed to address this crucial point.

VIII. CONCLUSION AND OUTLOOK

In this paper, we have investigated the application of the Carleman procedure to the Grad's formulation of generalized hydrodynamics. This analysis was motivated by previous works [11, 12], where we analysed the Carleman LB and the Carleman NS methods, respectively. The first (CLB) shows excellent convergence between the linearised and the classical solution for a large number of time steps, in the order of hundreds. However, its inherent nonlocality generates a number of Carleman variables which grows exponentially with the truncation order. As a result, the number of two-qubit quantum gates of the CLB circuit scales exponentially with the number of qubits.

The second method (CNS) can be written using a local formalism, thus allowing the number of Carleman variables to scale linearly with the number of lattice sites. However, the simulations show that a satisfactory convergence between the Carleman and the classical solution can be achieved only for a few timesteps. This is due to a number of reasons, not least the lack of unitarity of the time-marching scheme.

As expected, Carleman Grad sits somewhere in between. Our results show good convergence of the linearization method up to about thirty timesteps at $k = 5$ -th order of truncation, and the analysis of the quantum complexity points to potentially viable implementations using quantum linear solvers. However, the convergence horizon is still at least one order of magnitude too short for practical fluid-dynamic purposes.

Many directions for future work remain to be explored, such as the search of more efficient decompositions of the CLB matrix, as well as improvements of the convergence of the CG procedure by resorting to more advanced space and time discretization techniques, along with reduced sparse-matrix representations. Yet another direction is Carleman linearization based on orthogonal polynomials, such as Tsebitchev, which may significantly improve convergence. Only the future can tell which one will take us closer to a quantum algorithm for fluid flows.

ACKNOWLEDGEMENTS

The authors have benefited from valuable discussions with many colleagues, particularly M. Lauricella, R. Scatamacchia. The authors acknowledge financial support from the Italian National Centre for HPC, Big Data and Quantum Computing (CN00000013).

The authors have no conflicts to disclose. The data that support the findings of this study are available from the corresponding author upon reasonable request.

-
- [1] Ren Steijl. Quantum algorithms for fluid simulations. In *Advances in Quantum Communication and Information*. IntechOpen.
 - [2] Frank Gaitan. Finding flows of a navierstokes fluid through quantum computing. 6(1):1–6. Number: 1 Publisher: Nature Publishing Group.
 - [3] Rene Steijl. Quantum algorithms for nonlinear equations in fluid mechanics. In Yongli Zhao, editor, *Quantum Computing and Communications*. IntechOpen.
 - [4] Sauro Succi, W. Itani, K. Sreenivasan, and R. Steijl. Quantum computing for fluids: Where do we stand? 144(1):10001. Number: 1 Publisher: EDP Sciences, IOP Publishing and Societ Italiana di Fisica.
 - [5] Claudio Sanavio, Sauro Succi, Claudio Sanavio, and Sauro Succi. *Quantum Computing for Simulation of Fluid Dynamics*. IntechOpen.
 - [6] Sachin S. Bharadwaj and Katepalli R. Sreenivasan. Quantum computation of fluid dynamics. 3(1).
 - [7] Sauro Succi, Wael Itani, Claudio Sanavio, Katepalli R. Sreenivasan, and Ren Steijl. Ensemble fluid simulations on quantum computers. 270:106148.
 - [8] www.ibm.com/roadmaps/quantum.
 - [9] Michael Lubasch, Jaewoo Joo, Pierre Moinier, Martin Kiffner, and Dieter Jaksch. Variational quantum algorithms for nonlinear problems. 101(1):010301. Number: 1.
 - [10] Torsten Carleman. Application de la thorie des quations integrales lineaires aux systmes d'equations differentielles non lineaires. 59:63–87. Number: none Publisher: Institut Mittag-Leffler.
 - [11] Claudio Sanavio and Sauro Succi. Lattice boltzmann-carleman quantum algorithm and circuit for fluid flows at moderate reynolds number. 6(2):023802.
 - [12] C. Sanavio, R. Scatamacchia, C. de Falco, and S. Succi. Three carleman routes to the quantum simulation of classical fluids. 36(5):057143.
 - [13] Jin-Peng Liu, Herman ie Kolden, Hari K. Krovi, Nuno F. Loureiro, Konstantina Trivisa, and Andrew M. Childs. Efficient quantum algorithm for dissipative nonlinear differential equations. 118(35):e2026805118.
 - [14] Simone Melchionna, Massimo Bernaschi, Sauro Succi, Efthimios Kaxiras, Frank J. Rybicki, Dimitris Mitsouras, Ahmet U. Coskun, and Charles L. Feldman. Hydrokinetic approach to large-scale cardiovascular blood flow. 181(3):462–472.

- [15] Giacomo Falcucci, Giorgio Amati, Pierluigi Fanelli, Vesselin K. Krastev, Giovanni Polverino, Maurizio Porfiri, and Sauro Succi. Extreme flow simulations reveal skeletal adaptations of deep-sea sponges. 595(7868):537–541. Number: 7868 Publisher: Nature Publishing Group.
- [16] Sauro Succi. *The lattice Boltzmann equation: for complex states of flowing matter*. Oxford university press.
- [17] R. Benzi, S. Succi, and M. Vergassola. The lattice boltzmann equation: theory and applications. 222(3):145–197.
- [18] Wael Itani and Sauro Succi. Analysis of carleman linearization of lattice boltzmann. 7(1):24. Number: 1 Publisher: Multidisciplinary Digital Publishing Institute.
- [19] Xiangyu Li, Xiaolong Yin, Nathan Wiebe, Jaehun Chun, Gregory K. Schenter, Margaret S. Cheung, and Johannes Mlmensttdt. Potential quantum advantage for simulation of fluid dynamics. Issue: arXiv:2303.16550.
- [20] Harold Grad. Statistical mechanics, thermodynamics, and fluid dynamics of systems with an arbitrary number of integrals. 5(4):455–494.
- [21] Henning Struchtrup and Manuel Torrilhon. Regularization of grads 13 moment equations: Derivation and linear analysis. 15(9):2668–2680.
- [22] A. Mezzacapo, M. Sanz, L. Lamata, I. L. Egusquiza, S. Succi, and E. Solano. Quantum simulator for transport phenomena in fluid flows. 5(1):13153. Number: 1 Publisher: Nature Publishing Group.
- [23] Dominic W. Berry, Graeme Ahokas, Richard Cleve, and Barry C. Sanders. Efficient quantum algorithms for simulating sparse hamiltonians. 270(2):359–371. Number: 2.
- [24] Dominic W. Berry and Andrew M. Childs. Black-box hamiltonian simulation and unitary implementation. 12(1). Number: 1&2.
- [25] Aram W. Harrow, Avinatan Hassidim, and Seth Lloyd. Quantum algorithm for linear systems of equations. 103(15):150502. Number: 15.
- [26] Andrew M. Childs, Robin Kothari, and Rolando D. Somma. Quantum algorithm for systems of linear equations with exponentially improved dependence on precision. 46(6):1920–1950. Number: 6.
- [27] Ashley Montanaro and Sam Pallister. Quantum algorithms and the finite element method. 93(3):032324. Number: 3.

Appendix A: Explicit form of the Carleman-Grad matrices

In this Appendix, we provide the explicit form of the matrices A , B , and C of Eq. (25) for the case of a two-dimensional system. The Carleman vector at first order is defined as $V = (\rho, J_1, J_2, P_{11}, P_{12}, P_{22})$, and the components V_a are indexed with a running from 0 to 5.

The final result is:

$$A = dt \begin{pmatrix} 1/dt & \partial_1 & \partial_2 & 0 & 0 & 0 \\ 0 & 1/dt & 0 & \partial_1 & \partial_2 & 0 \\ 0 & 0 & 1/dt & 0 & \partial_1 & \partial_2 \\ \omega c_s^2 & -3c_2^2 \partial_1 & -c_s^2 \partial_2 & (1/dt - \omega) & 0 & 0 \\ 0 & -c_2^2 \partial_2 & -c_s^2 \partial_1 & 0 & (1/dt - \omega) & 0 \\ \omega c_s^2 & -c_2^2 \partial_1 & -3c_s^2 \partial_2 & 0 & 0 & (1/dt - \omega) \end{pmatrix}. \quad (\text{A1})$$

The matrices B and C are highly sparse, and the non-null components are

$$B_{311} = B_{412} = B_{522} = 2dt\omega, \quad (\text{A2})$$

$$C_{3110} = C_{4120} = C_{5220} = -dt\omega. \quad (\text{A3})$$

Usually, the derivative operators ∂_1, ∂_2 have to be converted to their discretized version D_1, D_2 , which are sparse matrices themselves. After naming the discretized version of the matrix A as \hat{A} , for a lattice with G gridpoints, this has the explicit form

$$\hat{A} = dt \begin{pmatrix} 1/dt & D_1 & D_2 & 0 & 0 & 0 \\ 0 & \mathbb{1}_N/dt & 0 & D_1 & D_2 & 0 \\ 0 & 0 & \mathbb{1}_N/dt & 0 & D_1 & D_2 \\ \omega c_s^2 \mathbb{1} & -3c_2^2 D_1 & -c_s^2 D_2 & (1/dt - \omega) \mathbb{1}_N & 0 & 0 \\ 0 & -c_2^2 D_2 & -c_s^2 D_1 & 0 & (1/dt - \omega) \mathbb{1}_N & 0 \\ \omega c_s^2 \mathbb{1}_N & -c_2^2 D_1 & -3c_s^2 D_2 & 0 & 0 & (1/dt - \omega) \mathbb{1}_N \end{pmatrix}, \quad (\text{A4})$$

where $\mathbf{1}_N$, D_1 and D_2 have dimension $N \times N$. The matrices B and C are changed into their N gridpoints version as

$$\begin{aligned}\hat{B} &= \mathbf{1}_N \otimes B \\ \hat{C} &= \mathbf{1}_N \otimes C.\end{aligned}\tag{A5}$$